Optical and electrical properties of electrochemically deposited polyaniline/CeO_2 hybrid nanocomposite film

Anees A. Ansari[1,†], M. A. M. Khan[1], M. Naziruddin Khan[1], Salman A. Alrokayan[1], M. Alhoshan[1,2], and M. S. Alsalhi[1]

[1]King Abdullah Institute for Nanotechnology, King Saud University, Riyadh-11451, P. O. Box-2454, Saudi Arabia
[2]Department of Chemical Engineering, King Saud University, P. O. Box 800, Riyadh 11421, Saudi Arabia

Abstract: This paper reports the optical and electrical properties of electrochemically deposited polyaniline (PANI)/cerium oxide (CeO_2) hybrid nano-composite film onto indium-tin-oxide (ITO) glass substrate. UV-visible spectroscopy and I–V characteristic were performed to study the optical and electrical parameters of the electrochemically deposited film. The film exhibited a strong absorption below 400 nm (3.10 eV) with a well defined absorbance peak at around 285 nm (4.35 eV). The estimated band gap of the CeO_2 sample was 3.44 eV, higher than bulk CeO_2 powder (E_g = 3.19 eV) due to the quantum confinement effect. Optical and electrochemical characteristics indicated that the electrical properties of PANI/CeO_2 hybrid nanocomposite film are dominated by PANI doping.

Key words: cerium oxide; polyaniline; nanocomposite; optical properties; electrical properties
DOI: 10.1088/1674-4926/32/4/043001 **EEACC:** 2520

1. Introduction

Recently, the synthesis of organic–inorganic hybrid nanocomposite materials has attracted substantial attention from many of the researchers because of the potential of combining distinct physical properties of organic and inorganic components within a single molecular composite[1−4]. Organic materials offer structural flexibility, convenient processing, tunable electronic properties, photoconductivity, efficient luminescence, and the potential for semiconducting and even metallic behavior. Inorganic metal nanoparticles provide the potential for high carrier mobilities, band gap tunability, a range of magnetic and dielectric properties, and thermal and mechanical stability. Besides this, conducting polymers, polyaniline (PANI), offer unique electrical conductivity, environmental stability and reversible electrochemical and physical properties, which can be controlled by its oxidation and protonation state[5−7]. These excellent novel features of the organic–inorganic hybrid nanocomposite materials greatly widen their applicability in the fields of catalysis, optoelectronic devices[5, 8], biosensors[2−6, 9−11], colloidal ink[12], energy storage devices and anticorrosion coatings[8,13]. In recent years, various successful strategies have been used for the fabrication of organic–inorganic hybrid nanocomposite films onto conducting glass electrode, including physical vapor deposition methods, layer-by-layer deposition, self-assembled monolayers, template synthesis and electrochemical polymerization deposition methods[4−11,14]. Among these reported approaches, electrochemical deposition is the most promising cost effective method with controllable film thickness and uniformity of the deposited film. The resulting hybrid nanocomposite films with controllable thickness and uniformity have shown promising prospective applications in solar cells, gas sensors and biosensors[2−11,14].

Among semiconductor metal oxides, CeO_2 has received great attention because of its unique features, including non-toxicity, biocompatibility, oxygen storage capability, electrocatalytic ability, optical, thermal properties, which have significant applications in solar cells, solid oxide fuel cells, gas sensors and biosensors[15−17]. Several reports are focused on polyaniline/metal oxide nanocomposites[18−22]. Xiong *et al.*[18] prepared PANI/TiO_2 hybrid microwires with diameters of 160–180 nm through the sol–gel process. The efficiency of photoelectric transformation of PANI/TiO_2 nanocomposites was higher than that of TiO_2 due to the sensitizing effect of PANI, which extends the absorption range of TiO_2. He *et al.*[19] synthesized PANI/nano-CeO_2 composite microspheres with an average diameter of 7 mm via a solid-stabilized emulsion (toluene/water emulsion) route. In another report[20] , a feasible method was proposed for the preparation of PANI/CeO_2 hybrid nanocomposites. The precursors of hybrid materials can form homogeneous dispersion. Moreover, the chemical interactions between the organic phase (PANI) and inorganic phase (CeO_2) in a hybrid system can maintain a small domain size and stable dispersion. If the hybrid process is introduced into a confined environment, e.g. template channel, the resulting materials must possess a special structure and properties. Ansari *et al.*[22] have developed a PANI/CeO_2 hybrid nanocomposite for fabrication of a hydrogen peroxide biosensor.

In the present paper, we discuss the optical and electrical properties of electrochemically deposited PANI/CeO_2 hybrid nanocomposite films on a conducting glass electrode for biosensing applications.

2. Experimental details

All chemicals, such as aniline, $(NH_4)_2Ce(NO_3)_6$, ethanol, NH_4OH and HNO_3, were of analytical grade and procured from

† Corresponding author. Email: aneesaansari@gmail.com
Received 3 October 2010, revised manuscript received 12 November 2010

Table 1. Optical parameters of PANI/CeO_2 film at 443 nm.

Sample	α (10^4 cm^{-1})	n	k	ε_r	ε_i	E_g (eV)
PANI/CeO_2/ITO	4.567	3.35	0.0161	11.22	0.011	3.32

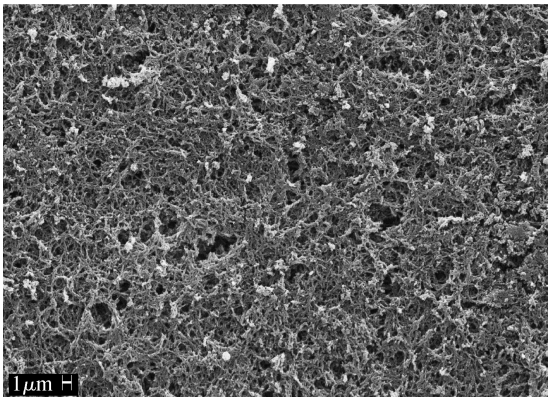

Fig. 1. SEM micrograph of PANI/CeO_2 the hybrid nanocomposite film.

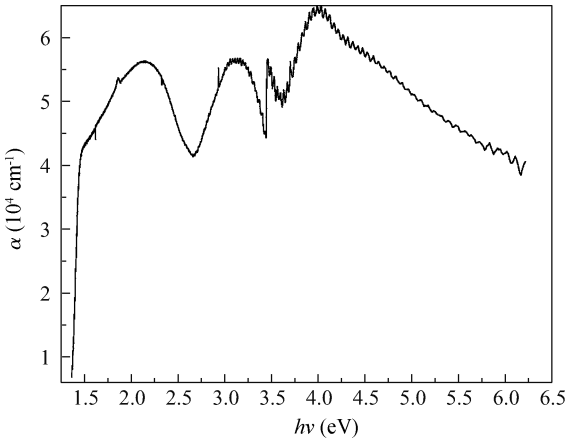

Fig. 2. Absorption coefficient α versus photon energy ($h\nu$) of the PANI/CeO_2 hybrid nanocomposite film.

Merck India Ltd, Mumbai, India. Aniline was distilled prior to use. The deionized water (phosphate buffer solution) obtained from a Millipore water purification system (Milli Q 10 TS) was used for the preparation of solutions and buffers.

CeO_2 nanoparticles were prepared by the co-precipitation method. PANI/CeO_2 hybrid nanocomposite film was deposited onto a conducting indium-tin-oxide (ITO) glass electrode by an electrochemical process, as discussed in an earlier report[22]. The PANI/CeO_2 hybrid nanocomposite electrode was characterized by UV-visible spectroscopy (Shimadzu UV-2100 spectrometer) in the range 200–900 nm. The morphology of the bioelectrode was studied using scanning electron microscopy [JSM-5600 LV(JEOL, Japan)]. Electrochemical characterization was carried out using an Auto-lab potentiostat/Galvanlstat (EcoChemie, Netherlands) using a three-electrode cell in phosphate buffer saline (PBS, 50 mM, pH 7.0, 0.9% NaCl) containing 5 mM$[Fe(CN)_6]^{3-/4-}$.

3. Results and discussion

The surface morphology of the deposited film was examined by scanning electron microscopy (SEM). The SEM micrograph displays a nano-fibrous network structure with high porosity, and interconnectivity enhances the electrical conductivity of the hybrid nanocomposite film (Fig. 1). The thickness of the deposited PANI-CeO_2 hybrid nanocomposite film was measured around 300 nm.

Figure 2 shows results of absorption spectra carried out by UV-visible spectroscopy on PANI/CeO_2 hybrid nanocomposite film measured in the range of 200–900 nm wavelengths. The absorption spectrum of PANI/CeO_2 hybrid nanocomposite shows three absorption bands at 325–360 nm, 400–430 nm and 780–825 nm that are attributed to π–π^* of benzenoid rings, polaron–bipolaron transition, and the benzenoid to quinoid excitonic transition, respectively. A strong absorption band at 780–875 nm appeared, which was due to the exciton transition of the quinoid rings. This result indicated that polyaniline completely transformed from the emeraldine salt to the emeraldine base form by the deprotonation of polyaniline with NH_4OH[7, 8]. Optical measurements constitute the most important means of determining the band structures of hybrid nanocomposite. The optical behavior of hybrid nanocomposite material is generally utilized to determine its optical constants e.g. refractive index (n) and extinction coefficient (k). To find these optical constants from the reflectance data obtained from the spectrophotometric measurements, the following relations are used[23, 24].

The absorption coefficient (α) of PANI/CeO_2 hybrid nanocomposite film was calculated using the well known relation

$$\alpha = \frac{1}{d} \ln \frac{1}{\omega}, \tag{1}$$

where d is the thickness of film and ω is the absorbance. The value of the absorption coefficient for PANI/CeO_2 hybrid nanocomposite film typically at 700 nm is listed in Table 1. The optical band gap and optical constants are studied as a function of photon energy for the PANI/CeO_2 hybrid nanocomposite film. Figure 2 shows the change in absorption coefficient (α) as a function of incident photon energy ($h\nu$) for nanocomposite film.

The absorption spectrum was applied to examine the effect of particle size on band gap energy of the PANI/CeO_2 hybrid nanocomposite film. The nanocomposite film distinctly exhibited broad bands that are attributed to π–π^* of benzenoid rings, polaron–bipolaron transition, and the benzenoid to quinoid excitonic transition, respectively. The band gap energy, E_g for hybrid nanocomposite film is determined by fitting the absorption data to the direct transition equation by extrapolating the linear portions of the curves to absorption equal to zero (Fig. 3),

$$\alpha = \frac{2.303 \times 10^3 A\rho}{lC}, \tag{2}$$

where A is the absorbance of a sample, ρ the density of the

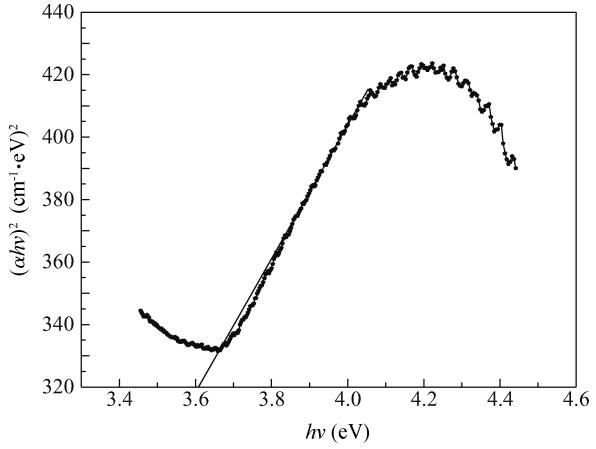

Fig. 3. Plot of $(\alpha h\nu)^2$ versus photon energy ($h\nu$) of the PANI/CeO_2 hybrid nanocomposite film.

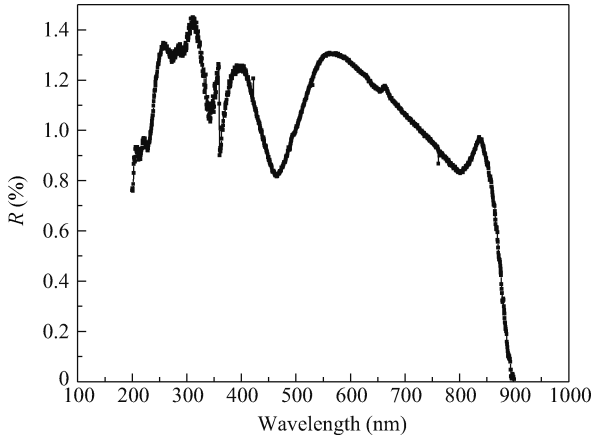

Fig. 4. Optical reflectance (R) with wavelength spectra of the PANI/CeO_2 hybrid nanocomposite film.

PANI/CeO_2 hybrid nanocomposite film (7.28 g/cm^3), C the particle loading in g/L, and l the path length. The optical absorption coefficient α near the absorption edge for the inter band transitions was obtained using the models proposed by Mot and Davis[25],

$$\alpha = \frac{B(h\nu - E_g)^n}{h\nu}, \tag{3}$$

where B is a constant, E_g the optical band gap, α the absorption coefficient, $h\nu$ the photon energy, and n a refractive index that can assume values of 0.5, 1.5, 2 and 3, depending on the nature of the electronic transitions responsible for the absorption[26]. n is equal to 0.5 for allowed direct transitions, 1.5 for forbidden direct transitions, 2 for allowed indirect transitions and 3 for forbidden indirect transitions. The energy intercept of a plot of $(\alpha h\nu)^2$ versus $h\nu$ yields E_d for the allowed direct transition (n = 1/2), and the energy intercept of a plot of $(\alpha h\nu)^{1/2}$ versus $h\nu$ yield E_i for the allowed indirect transition (n = 2). The PANI/CeO_2 hybrid nanocomposite shows a strong absorption below 400 nm (3.10 eV) with a well-defined absorption peak at around 285 nm (4.35 eV). The estimated band gap of the hybrid nanocomposite is 3.10 eV, which is closely matched with the earlier published report by Yin *et al.*[27] (E_g = 3.03–3.68 eV for CeO_2 nanoparticles synthesized using sonochemical synthesis). Ho *et al.*[28] (E_g = 3.36–3.62 eV for mesoporous CeO_2 nanostructures prepared using a polyol method), and Chen and Chang[29] (E_g = 3.56–3.71 eV for CeO_2 nanoparticles prepared using a precipitation method). It can be seen that the PANI/CeO_2 hybrid nanocomposite shows an increase in E_g value compared to the bulk CeO_2 powder (E_g = 4.35 eV, determined by UV-vis spectroscopy)[22, 30]. The increase in band gap with CeO_2 concentration implies that the electronic structure of PANI is affected by CeO_2. So far, two kinds of explanation about the cause of increase in optical band gap of CeO_2 have been proposed. These include (1) the quantum confinement effect when the particle is down to a few nanometers and (2) the charge transition of Ce ion when the particle diameters are larger than a few nanometers (e.g. $\geqslant$ 8 nm)[31].

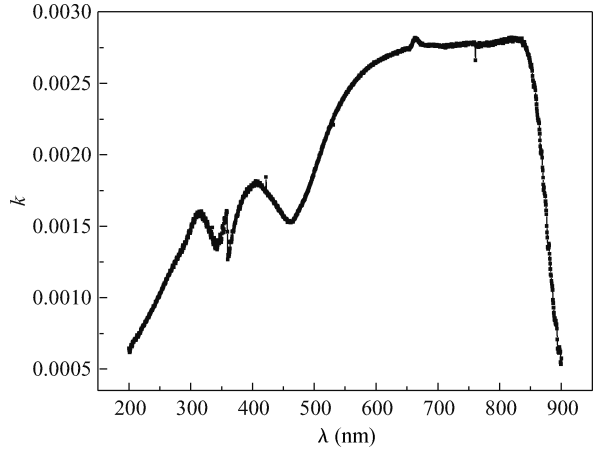

Fig. 5. Extinction coefficient (k) versus wavelength (λ) of the PANI/CeO_2 hybrid nanocomposite film.

The optical band gap, refractive index and extinction coefficient are the important parameters that are used to study the optical properties of the materials (Figs. 4 and 5). The values of the refractive index (n) and extinction coefficient (k) were calculated using the theory of reflectivity of light. According to this theory, the reflectance of light from a film can be expressed in term of Fresnel's coefficient. The reflectivity[24] on an interface can be given by

$$R = \frac{[(n-1)^2 + k^2]}{[(n+1)^2 + k^2]}, \tag{4}$$

and

$$\alpha = \frac{4\pi k}{\lambda}. \tag{5}$$

The dispersion relations of the refractive index n and k of the thin films are calculated using Eqs. (4) and (5). The values of n and k for the PANI/CeO_2 hybrid nanocomposite film are given in Table 1.

The relative permittivity of incident light for optical materials is the key parameter to determine their real (ε_r) and imaginary (ε_i) dielectrics constants (Fig. 5). These two optical parameters of these systems are evaluated with the help of the average refractive index n and the average extinction coefficient k[32] using the following relations,

$$\varepsilon_r = n^2 - k^2, \tag{6}$$

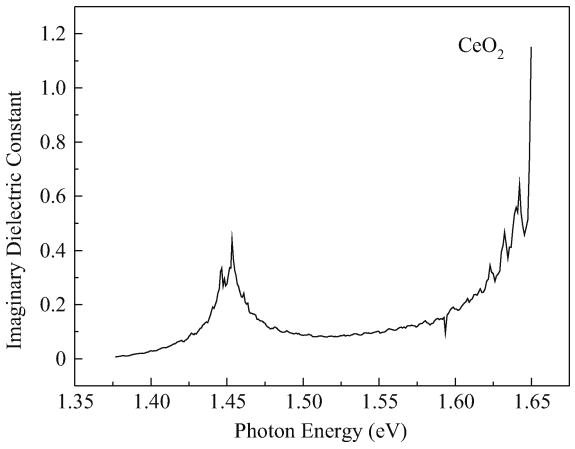

Fig. 6. Dielectric function of the PANI/CeO_2 nanocomposite film curves versus photon energy.

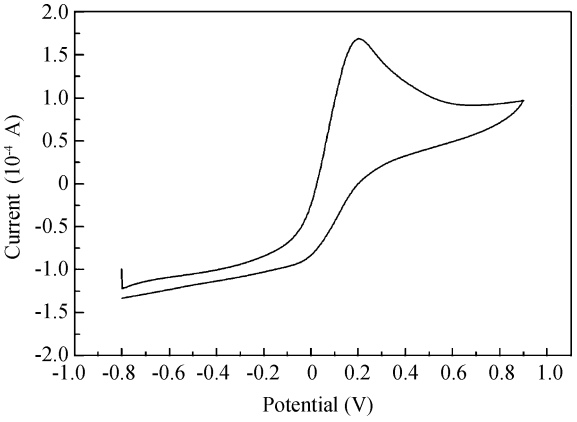

Fig. 7. Current versus potential (V) curves of the PANI/CeO_2 nanocomposite film.

and

$$\varepsilon_i = 2nk. \tag{7}$$

The values of these two parameters with fixed photon energy are given in Table 1. It can be seen that both the real part ε_r and the imaginary part ε_i of the dielectric constant decreases with increasing photon energy for the PANI/CeO_2 hybrid nanocomposite film (Fig. 6). The PANI/CeO_2 hybrid nanocomposite film shows improved optical characteristics as compared to the CeO_2 nanostructured films due to CeO_2 nanoparticles being loosely attached to the polymer chain by weak van der Waals forces of attraction.

4. Electrical studies

In order to determine the dominant transport mechanisms, current–voltage (I–V) measurements were recorded on a number of samples of PANI/CeO_2 electrode in phosphate buffer (50 mM, pH 7.0, 0.9% NaCl) at various scan rates from 10 to 100 mV/s and shown in Figs. 7 and 8. Dominant electrical transport mechanisms can be evaluated through standard Schottky barrier theory by the following expression[33]. The standard Schottky barrier theory should explain the saturation current J_S of

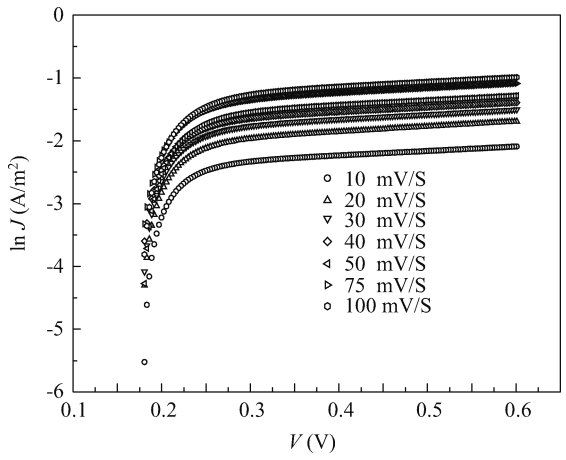

Fig. 8. ln J versus voltage of the PANI/CeO_2 hybrid nanocomposite film.

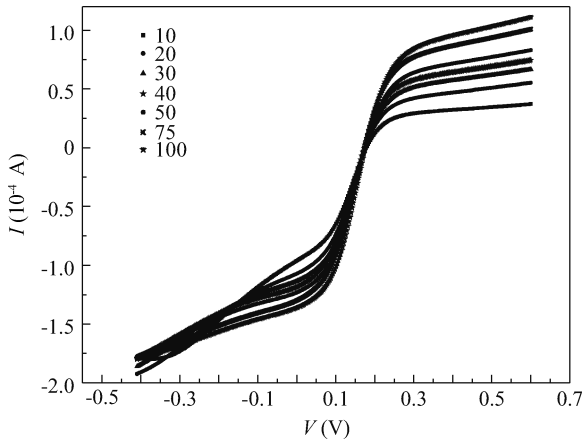

Fig. 9. Current versus voltage of the PANI/CeO_2 hybrid nanocomposite film.

the general I–V characteristics as a function of temperature T (room temperature) according to

$$J = J_S[\exp(qV/\eta kT) - 1], \tag{8}$$

where J is the instantaneous current density, J_S is the saturation current density, V is the applied potential, η is the ideality factor, q is the electronic charge, and k is the Boltzmann constant. The saturation current density J_S can be expressed as

$$J_S = A^*T^2\exp(-q\Phi_B/kT), \tag{9}$$

where $A^* = 4\pi m^* qk^2h^{-3}$ is the effective Richardson constant for thermionic emission corresponding to electron effective mass m^* in the semiconductor and h is the Plank constant.

The barrier height, Φ_B is the energy difference between the edge of the conduction band and the redox Fermi level of the electrolyte. This potential prevents most of the photo-generated charge carriers (electrons or holes) from passing from one to the other. However, these carriers under a biasing potential can get enough energy to cross the barrier. The barrier height Φ_B at the injected electrode is calculated by

$$\Phi_B = (kT/q)\ln(A^*T^2/J_S). \tag{10}$$

Table 2. Electrical parameters of the PANI/CeO_2 electrode.

Electrode scan rate (mV/s)	H	$\phi\,(V)$	R_c (mΩ)	J_s
10	1.87	0.664	2.7	0.28
20	1.73	0.657	2.3	0.37
30	1.64	0.656	2.1	0.39
40	1.51	0.654	2.9	0.41
50	1.33	0.653	2.7	0.42
100	1.17	0.651	2.8	0.48

The slopes of the linear portions of these curves were calculated and the ideality factors determined using the relation

$$\eta = \frac{1}{2.3026 \times \dfrac{kT}{q} \times \mathrm{d}(\lg I)/\mathrm{d}V}. \tag{11}$$

It has been observed that the ideality factor (η) and the apparent barrier height (Φ_B) increase with decrease in scan rate. On the other hand, the saturation current density J_s increases with increase in scan rate. Contact resistance has been evaluated using a current versus potential graph, as shown in Fig. 9 and found to be very low.

The reverse saturation current density J_S is obtained by dividing the reverse saturation current J by the geometrical area of the Schottky contact. The variation in J_S, along with n and Φ_B, with respect to the scan rates is shown in Table 2. The reverse bias I–V characteristics give information about the properties of the metal–semiconductor (MS) contact. The reserve current arises due to the recombination of charge carriers, the release of charge carriers from trap levels, the barrier lowering at high electric field or leakage. Hence the leakage current in the fabricated Schottky diode is of low value, which is indicative of its good quality.

The various factors may be responsible for these large variations observed in ideality factor and apparent barrier height with different scan rates. Some authors have explained these variations by using Fermi level pinning at the MS interface. The Fermi level pinning may occur either by metal induced gap states[34] or interface defects[35]. The dependence of Schottky barrier height (SBH) on temperature can give an insight into the physical mechanism of the Fermi level pinning in MS contacts. But in our case the variation in SBH with scan rates could be explained with the Fermi level pinning either by metal induced gap states (MIGS) or defect states. If the Fermi level pinning is due to MIGS, the scan rate dependence of SBH is governed by the scan rate dependence of the band gap. Thus, our results suggest that an inhomogeneous Schottky contact may behave like a high barrier contact.

Cyclic voltammograms experimental results suggested that the PANI/CeO_2 hybrid nanocomposite is an electroactive material that presents very stable electrochemical behavior in respect to the cerium oxide nanostructured film. This hybrid nanocomposite had shown better electrochemical properties, such as charge capacity, than cerium oxide nanoparticles. This geometry of the polymer is favorable for enhanced mobility of the CeO_2 ion or the charge transfer across the polymer chains and it enhances the conductivity of the hybrid nanocomposite material.

5. Conclusions

PANI/CeO_2 hybrid nano-composite film was prepared by *in situ* electrochemical polymerization of polyaniline by dispersing CeO_2 nanoparticles in the solution mixture. The results of the PANI/CeO_2 nanocomposite film were interpreted in terms of polarons and bipolarons and their contribution towards conductivity and dielectric relaxation. Due to the presence of cerium oxide in the polyaniline matrix, a significant enhancement in optical and electrochemical spectra was observed. SEM imaging proves the preparation of nanofibers of nanocomposite on the electrode surface. UV/Vis and electrochemical spectra confirm that there is strong chemical interaction between PANI and CeO_2. We expect that these optical and electrochemical properties of the deposited film will be applicable in the development of electrochemical nanodevices.

References

[1] Zou H, Wu S, Shen J. Polymer/silica nanocomposites: preparation, characterization, properties, and applications. Chem Rev, 2008, 108(9): 3893
[2] Hatchett D W, Josowicz M. Composites of intrinsically conducting polymers as sensing nanomaterials. Chem Rev, 2008, 108(2): 746
[3] Nastase C, Nastase F, Vaseashta A, et al. Nanocomposites based on functionalized nanotubes in polyaniline matrix by plasma polymerization. Prog Solid State Chem, 2006, 34(2–4):181
[4] Rajesh, Ahuja T, Kumar D. Recent progress in the development of nano-structured conducting polymers/nanocomposites for sensor applications. Sensors and Actuators B, 2009, 136(1): 275
[5] Malinauskas A, Malinauskiene J, Ramanavicius A. Conducting polymer-based nanostructurized materials: electrochemical aspects. Nanotechnology, 2005, 16(10): R51
[6] Peng H, Zhang L, Soeller C, et al. Conducting polymers for electrochemical DNA sensing. Biomaterials, 2009, 30(11): 2132
[7] Zhu C L, Chou S W, He S F, et al. Synthesis of core/shell metal oxide/polyaniline nanocomposites and hollow polyaniline capsules. Nanotechnology, 2007, 18(27): 275604
[8] Hussain F, Hojjati M, Okamoto M, et al. Polymer-matrix nanocomposites, processing, manufacturing, and application: an overview. Journal of Composite Materials, 2006, 40(17): 1511
[9] Abu-Salah K M, Alrokyan S A, Khan M N, et al. Nanomaterials as analytical tools for genosensors. Sensors, 2010, 10(1): 963
[10] Ansari A A, Alhoshan M, Alsalhi M S, et al. Nanostructured metal oxides based enzymatic electrochemical biosensors. In: Intelligent and Biosensors. Chapter 4. IN-TECH, 2009
[11] Ansari A A, Solanki P R, Kaushik A, et al. Recent advances in nanostructured metal oxides based electrochemical biosensors for clinical diagnostics. In: Yopgeshwaran U, Kumar S, Chen S, ed. Nanostructured materials for electrochemical biosensors. Chapter 7. Nova Science Publishers Inc. USA, 2009
[12] Zhang X, Manohar S K. Polyaniline nanofibers: chemical synthesis using surfactants. Chem Commun, 2004, (20): 2360
[13] Sotiropoulou S, Sastre Y S, Mark S S, et al. Biotemplated nanostructured materials. Chem Mater, 2008, 20(3): 821
[14] Ansari A A, Khan M N, Hoshan M Al, et al. Nanostructured materials: classification, properties, fabrication, characterization and their applications in biomedical sciences. In: Kestell A E, DeLorey G T, ed. Nanoparticles properties, classification, characterization, and fabrication. Nova Science Publishers Inc. USA, 2010
[15] Ansari A A, Solanki P R, Malhotra B D. Sol–gel derived nanostructured cerium oxide film for glucose sensor. Appl Phys Lett,

2008, 92(26): 263901
[16] Ansari A A, Solanki P R, Malhotra B D. Hydrogen peroxide sensor based on horseradish peroxidase immobilized nanostructured cerium oxide film. J Biotech, 2009, 142(2):179
[17] Ansari A A, Kaushik A, Solanki P R, et al. Sol–gel derived nanoporous cerium oxide film for application to cholesterol biosensor. Electrochem Commun, 2008, 10(9): 1246
[18] Xiong S, Wang Q, Chen Y, et al. Preparation of polyaniline/TiO_2 hybrid microwires in the microchannels of a template. Mater Chem Phys, 2007, 103(2/3): 450
[19] He Y. Synthesis of polyaniline/nano-CeO_2 composite microspheres via a solid-stabilized emulsion route. Mater Chem Phys, 2005, 92(1): 134
[20] Parvatikar N, Jain S, Bhoraskar S V, et al. Spectroscopic and electrical properties of polyaniline/CeO_2 composites and their application as humidity sensor. J Appl Poly Sci, 2006, 102(6): 5533
[21] Malta M, Louarn G, Errien N, et al. Nanofibers composite vanadium oxide/polyaniline: synthesis and characterization of an electroactive anisotropic structure. Electrochem Commun, 2003, 5(12): 1011
[22] Ansari A A, Sumana G, Khan R, et al. Polyaniline-cerium oxide nano-composite for hydrogen peroxide sensor. J Nanosci Nanotechnol, 2009, 9(8): 4679
[23] Patsalas P, Logothetidis S, Sygellou L, et al. Structure-dependent electronic properties of nanocrystalline cerium oxide films. Phys Rev B, 2003, 68(3): 035104
[24] Tauc J. Amorphous and liquid semiconductors. New York: Plenum Press, 1979: 159
[25] Mott N F, Davis E A. Electronic processes in non-crystalline materials. Oxford: Clarendon Press, 1979: 382
[26] Masui T, Fujiwara K, Machida K, et al. Characterization of cerium (IV) oxide ultrafine particles prepared using reversed micelles. Chem Mater, 1997, 9(10): 2197
[27] Yin L, Wang Y, Pang G, et al. Sonochemical synthesis of cerium oxide nanoparticles-effect of additives and quantum size effect. J Colloid Inter Sci, 2002, 246(1): 78
[28] Ho C, Yu J C, Kwong T, et al. Morphology-controllable synthesis of mesoporous CeO_2 nano- and microstructures. Chem Mater, 2005, 17(17): 4514
[29] Chen H I, Chang H Y. Synthesis of nanocrystalline cerium oxide particles by the precipitation method. Ceramic International, 2005, 31(6): 795
[30] Zhou K B, Wang X, Sun X M, et al. Enhanced catalytic activity of ceria nanorods from well-defined reactive crystal planes. J Cataly, 2005, 229(1): 206
[31] Mai H X, Sun L D, Zhang Y W, et al. Shape-selective synthesis and oxygen storage behavior of ceria nanopolyhedra, nanorods, and nanocubes. J Phys Chem B, 2005, 109(51): 24380
[32] Pandey V, Tripathi S K, Kumar A. Effect of in incorporation on optical properties of amorphous Se–Ge thin films. Physica B, 2007, 388(1/2): 200
[33] Gupta H M. Theory of electrical characteristics of a Schottky barrier having exponentially distributed impurity states and metal-insulator-metal structures. J Phys: Condens Matter, 1992, 4(13): 3507
[34] Tersoff J, Harrison W A. Transition-metal impurities in semiconductors—their connection with band lineups and Schottky barriers. Phys Rev Lett, 1987, 58(22): 2367
[35] Bardeen J. Surface states and rectification at a metal semiconductor contact. Phys Rev, 1947, 71(10): 717